


Air Fixation and AFM: A Comparative Study of Nanoparticle-Induced Topographical Changes in Lung Cells

Gamze Yeşilay^{1,2} 

¹ University of Health Sciences, Experimental Medicine Application & Research Center, Validebag Research Park, Türkiye, gamze.yesilay@sbu.edu.tr

² Department of Molecular Biology and Genetics, Hamidiye Institute of Health Sciences, University of Health Sciences, Türkiye

ARTICLE INFO

ABSTRACT

Keywords:
Desiccation
Sample preparation
Membrane roughness



Article History:
Received: 21.06.2024
Accepted: 14.10.202
Online Available: 23.10.2024

Gold nanoparticles (AuNPs) have emerged as promising agents in biomedical applications due to their unique physicochemical properties. This study investigates the cellular interactions of AuNPs with A549 (non-small cell lung adenocarcinoma) and BEAS-2B (normal bronchial epithelial) cell lines. AuNPs were synthesized via the citrate reduction method, resulting in 20, 50, and 70 nm particles.

Cells were incubated with AuNPs for increasing durations (30 minutes, 4 hours, and 24 hours). Post-incubation, cells were washed with PBS, air-fixed, and subsequently analyzed using Atomic Force Microscopy (AFM) to obtain detailed topographical maps. AFM imaging revealed distinct interactions between AuNPs and the two cell lines.

A549 cells displayed darker regions on the cell surface, indicative of topographical depressions likely resulting from nanoparticle-induced membrane collapse. In contrast, BEAS-2B cells did not exhibit such depressions, which is consistent with the literature that suggests cancer cells are mechanically softer than normal cells.

The surface roughness analysis results indicated that the preservation of surface integrity post-fixation validates the air-fixation methodology for obtaining reliable mechanical data from AFM analyses.

1. Introduction

Atomic Force Microscopy (AFM) has emerged as a critical tool for cellular imaging, providing high-resolution topographic maps of cell surfaces and offering significant insights into cellular morphology, mechanical properties, and surface roughness [1, 2]. The ability of this technique to capture nanometer-scale features makes it indispensable for understanding cellular processes and interactions, particularly in cancer research, as cancer cells exhibit unique mechanical properties, such as reduced stiffness and altered surface topography, compared to their normal counterparts [3]. Gaining insight on these subtle changes is essential for understanding cancer progression and developing new diagnostic approaches. At this

point, sample preparation step for AFM is critical. Among various sample preparation methods, air fixation of cells offers unique advantages over conventional chemical fixation and live-cell AFM imaging in terms of preserving surface integrity and reducing artifacts [4, 5].

Chemical fixation methods, such as formaldehyde or glutaraldehyde, are commonly used to stabilize cellular structures for AFM imaging. These fixatives cross-link proteins and other cellular components, "freezing" the cells in a state closely resembling their natural conditions. However, chemical fixation can create artifacts due to potential over-fixation or uneven penetration, which may alter the natural topography of the cell surface [6]. Additionally,

residual chemicals can sometimes interfere with subsequent AFM imaging and analysis.

On the other hand, live-cell AFM imaging allows the real-time observation of dynamic cellular processes. This method provides valuable insights into cell mechanics and behaviors under physiological conditions. However, maintaining cell viability during imaging can be challenging and requires complex environmental control systems to maintain optimal temperature, CO₂ levels, and humidity [7]. Moreover, live-cell imaging is sensitive to thermal drift and noise, which can compromise the resolution needed to detect fine topographical changes, such as membrane roughness or indentation patterns induced by nanoparticles.

Air fixation, a less invasive and artifact-free alternative, has shown promise in preserving cellular structures while enabling high-resolution AFM imaging. This method avoids the chemical distortions introduced by traditional fixation techniques and provides stable samples suitable for detailed surface roughness and topography analyses [4, 5]. Given that membrane roughness is a critical indicator of cellular mechanical properties, particularly in distinguishing cancerous cells from normal ones, there is a need for more accurate and non-invasive fixation methods that can retain the native surface characteristics of cells.

Gold nanoparticles (AuNPs) are increasingly recognized for their potential in biomedical applications, particularly in cancer diagnosis and treatment, due to their unique physicochemical properties. The cellular interactions of AuNPs, especially their impact on the cell membrane's mechanical properties, remain a key area of research [8]. Specifically, understanding how AuNPs induce topographical and roughness changes in cancerous versus normal cells can provide valuable insights into cancer cell behavior, as cancer cells are known to be mechanically softer than their normal counterparts [3].

In this study, the applicability of air fixation as a method for preserving the native membrane structures of both cancerous and normal lung cells was explored, with the aim of assessing its

potential to enable precise AFM measurements of surface roughness and topographical changes. Specifically, the effects of AuNPs of increasing diameter sizes (20 nm, 50 nm, and 70 nm) on A549 (non-small cell lung adenocarcinoma) and BEAS-2B (normal bronchial epithelial) cell lines.

The hypothesis is that the surface roughness changes induced by AuNPs will differ between cancerous and normal cells, with more pronounced changes in A549 cells due to their altered membrane mechanics. It was also aimed to determine whether air fixation can effectively reveal these subtle surface alterations and differential AuNP uptake between the two cell lines. The cell lines were incubated with AuNPs for different time points (30 minutes, 4 hours, and 24 hours), air-fixed, and then analyzed using AFM. The time-dependent topographic changes caused by increasing AuNP diameter sizes in air-fixed cell samples were evaluated.

2. General Methods

2.1. AuNP synthesis

AuNPs were synthesized using the citrate reduction method [9]. Initially, for the synthesis of 20 nm AuNPs, 10 mg of HAuCl₄·3H₂O was dissolved in 100 mL of deionized water. Upon the solution reaching a boil, 2 mL of a 1% sodium citrate (w/v) solution was rapidly added while stirring. The solution was continuously stirred at boiling temperature until a deep red color was observed. To synthesize larger AuNPs, the amount added from sodium citrate (1%, w/v) was adjusted to 0.8 mL for 50 nm AuNPs and 0.6 mL for 70 nm AuNPs. UV-Visible spectroscopy (Shimadzu, UV3600i Plus) was used to confirm the characteristic plasmon resonance peaks of the synthesized AuNPs. Dynamic Light Scattering (DLS) (Malvern, ZetaSizer Ultra) was used to verify the size and distribution of AuNPs.

2.2. Cell culture

BEAS-2B cell line was cultured in Dulbecco's Modified Eagle Medium (DMEM), while A549 cells were cultured in DMEM-F12 medium. Both media were supplemented with 10% fetal bovine serum (FBS) and 1% penicillin-streptomycin.

Cells were maintained at 37°C in a humid atmosphere with 5% CO₂.

For A549 cell line, 7500 cells were seeded on each round coverslip, and for the BEAS-2B cell line, 5000 cells were seeded on each coverslip. The coverslips were placed in 24-well plates and allowed to grow until they reached 80% confluency. All experiments were performed in triplicate. Cells were incubated with AuNPs at a concentration of 50 µg/mL for three different time points: 30 minutes, 4 hours, and 24 hours. Post-incubation, cells were thoroughly washed with PBS to remove uninternalized AuNPs and air-fixed in a desiccator for 24 hours. The next day, dried cells were washed with deionized water to remove salts from PBS and then re-dried for AFM imaging.

2.3. AFM imaging

Fixed cells were imaged using a Nanosurf CoreAFM. Imaging was conducted with a PPP-NCLR (Nanosurf) cantilever in tapping mode to obtain detailed topographic maps of cell surfaces. Each scan consisted of 512 points per line at a scan rate of 1 line per second. Three 100×100 µm² areas were scanned for each sample.

2.4. Surface roughness analysis

Surface roughness parameters and standard deviation parameters were calculated using Gwyddion 2.66 open-source software. Pre-processing steps applied to the AFM images included leveling data by mean plane subtraction, polynomial row alignment, measurement range normalization, and image sharpening using Laplacian filtering.

3. Results and Discussion

3.1. AuNP characterization

UV-Visible spectra and DLS results of the AuNPs confirm that the synthesis achieved the targeted sizes (Figure 1).

The synthesized AuNPs match the size-absorbance peak results reported in the literature (Figure 1A) [10]. Additionally, the hydrodynamic diameter measurements obtained

using DLS confirm that the targeted AuNP sizes were achieved (Figure 1B).

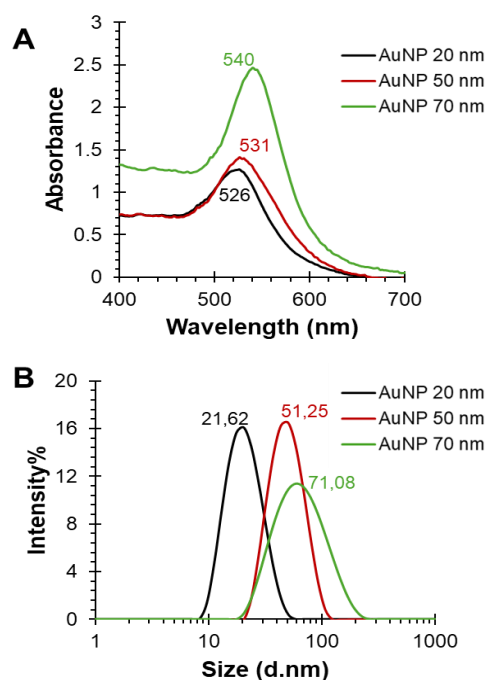


Figure 1. AuNP characterization results. (A) UV-Visible spectra and absorbance peaks. (B) DLS distribution and hydrodynamic diameter results.

3.2. AFM imaging

AFM topography images were obtained after the interaction of AuNPs with increasing diameters with both cell lines at increasing time points (Figures 2 and 3).

Figure 2 presents the AFM images of A549 cells incubated with AuNPs of increasing diameters and varying time points. Panel (A) shows the control sample without AuNP treatment, providing a baseline reference for cellular surface topography. Panels (B-D) display the topographical changes after 30 minutes of incubation with 20 nm, 50 nm, and 70 nm AuNPs, respectively, while panels (E-G) and (H-J) depict the topographical changes after 4 hours and 24 hours of incubation. The darker regions observed in A549 cell line represent topographical changes and cellular responses resulting from the interaction of nanoparticles with the cell surface (Figure 2).

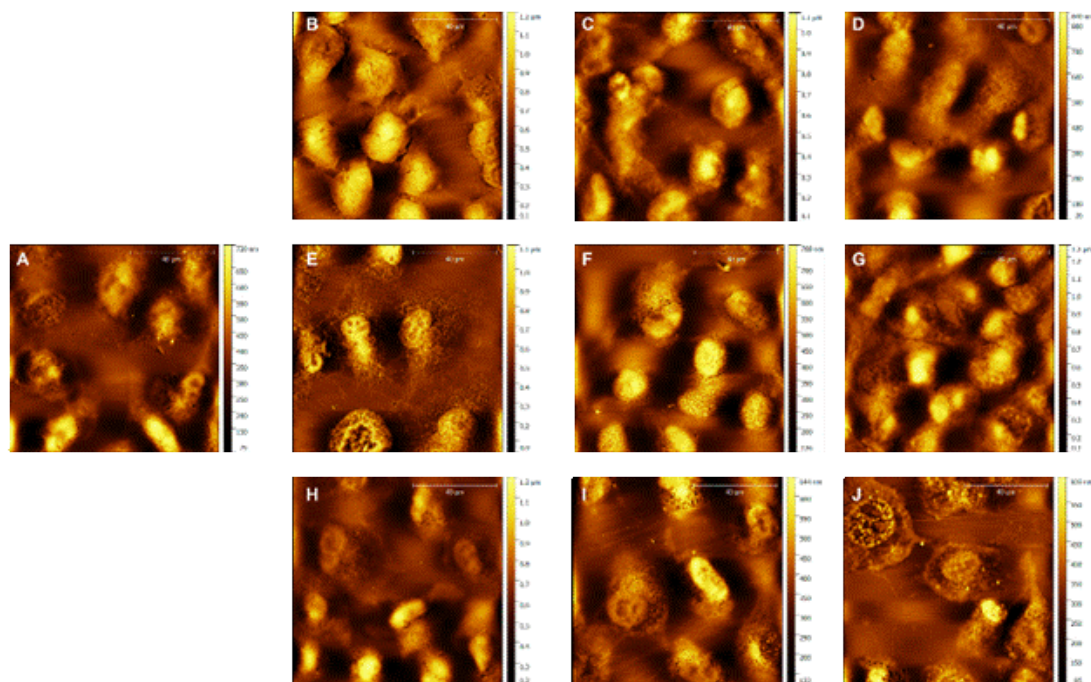


Figure 2. AFM images obtained for A549 cell line based on increasing AuNP diameters and incubation times. (A) Control sample not treated with AuNP. (B-D) Images obtained after incubation with AuNP for 30 minutes, (E-G) 4 hours, and (H-J) 24 hours. Images for samples incubated with (B, E, H) 20 nm AuNPs, (C, F, I) 50 nm AuNPs, and (D, G, J) 70 nm AuNPs. Scale bars are 40 µm.

The membrane structure observed in the BEAS-2B cell line in the control group and other samples shows significant differences compared to A549 cell line (Figure 3). As indicated in the literature, cancer cells have a mechanically "softer" structure compared to normal cells,

leading to indentations in A549 cell line, while such topographical changes are not observed in BEAS-2B cell line [11].

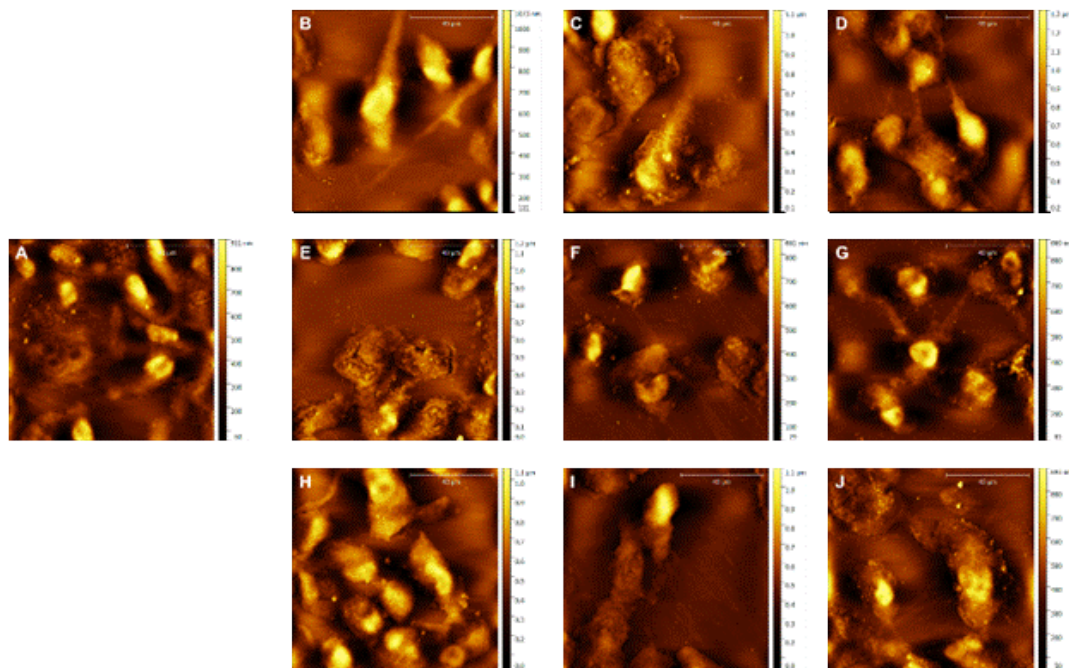


Figure 3. AFM images obtained for the BEAS-2B cell line based on increasing AuNP diameters and incubation times. (A) Control sample not treated with AuNP. (B-D) Images obtained after incubation with AuNP for 30 minutes, (E-G) 4 hours, and (H-J) 24 hours. Images for samples incubated with (B, E, H) 20 nm AuNPs, (C, F, I) 50 nm AuNPs, and (D, G, J) 70 nm AuNPs. Scale bars are 40 µm.

For both cell lines, the data shows that when AuNPs bind to or are internalized by the cell surface, they cause indentations or flattening in specific areas of the cell membrane. The presence of nanoparticles on the cell surface can induce morphological changes such as resorption, making certain areas of the cell membrane appear thinner or collapsed [12]. These effects are observed as darker regions in AFM images (Figure 2B-J, Figure 3B-J) representing topographical depressions or lower elevations, which are most likely caused by nanoparticle-induced membrane deformation. These depressions are more pronounced in samples incubated with 20 nm AuNPs (panels B, E, H), which aligns with the hypothesis that smaller nanoparticles induce more significant surface alterations due to higher cellular uptake. As incubation time increases (panels H-J), the topographical features become less pronounced, suggesting that the nanoparticles are being internalized, leading to a reduction in surface roughness. This temporal trend supports the notion that AuNP interactions with the cell membrane evolve over time, causing initial membrane deformation followed by nanoparticle uptake.

As seen in the figures, the surface integrity of the samples examined after air fixation was preserved and suitable for obtaining mechanical information.

3.3. AFM roughness analysis

The effect of AuNPs on the surface roughness of A549 and BEAS-2B cell lines was investigated using three important roughness parameters: arithmetic mean roughness (Ra), root mean square roughness (Rq), and maximum profile height (Rt). The results provide detailed information on the topographical changes caused by increasing AuNP sizes (20 nm, 50 nm, and 70 nm) over increasing incubation times (30 minutes, 4 hours, and 24 hours) (Table 1).

The basic roughness parameters of the control samples not treated with AuNPs (CtrlA and CtrlB) reveal inherent differences in surface topography between cancerous and non-cancerous cells. BEAS-2B cell line (CtrlB) exhibits higher basic roughness compared to

A549 cell line (CtrlA), indicating that normal lung epithelial cells have a more irregular surface. This could be attributed to the altered membrane properties of cancer cells, which may facilitate higher interaction or uptake rates of AuNPs in A549 cell line. In contrast, BEAS-2B cell line shows more variability in roughness parameters with larger AuNPs and longer incubation times, reflecting different interaction dynamics.

Table 1. Ra, Rq, and Rt values obtained from AFM measurements. (Ctrl: sample not treated with AuNP, other groups' names represent the incubation time (30 min, 4 h, 24 h), AuNP diameter (20, 50, 70 nm), and cell line (A549, BEAS-2B) respectively.)

	Ra	Rq	Rt
CtrlA	70.53±27.73	91.08±34.87	358.3±116.6
3020A	116.4±37.55	151.4±50.97	674.3±203.8
0420A	130.1±57.85	174.8±62.12	828±318.7
2420A	105.9±53.95	141.1±59.8	538.8±240.6
3050A	117.7±41.27	148.6±48.58	609.8±162.2
0450A	92.29±33.5	117.1±35.81	481.9±141
2450A	63.37±27.19	83.59±31.56	336.5±133.5
3070A	74.86±24.71	97.78±30.3	410.6±118.6
0470A	121.8±29.81	152±36.36	611.5±129.7
2470A	43.7±12.96	60.66±21.52	317.1±97.7
CtrlB	79.72±34.26	105.4±45.27	424.5±158
3020B	85.17±48.15	117.5±51.14	404.7±220.6
0420B	115.2±51.89	156.8±67.98	763.9±314.2
2420B	113.4±23	138.4±25.65	528.6±98.17
3050B	89.36±47.46	126.4±57.13	506.1±271.7
0450B	77.98±43.5	111.1±46.69	421.6±247.7
2450B	97.94±59.99	135.9±85.43	472.6±240.7
3070B	102.5±64.98	144.2±76.27	509.5±277.1
0470B	93.44±52.49	126.7±56.69	444.2±234.2
2470B	69.14±23.63	92.43±31.82	419.4±145.1

Small AuNPs (20 nm) caused the most significant changes in surface roughness for both cell lines. In A549 cell line, Ra, Rq, and Rt values significantly increased after 4 hours of incubation, indicating a high density of AuNPs on the cell membrane surface. This trend is also observed in BEAS-2B cell line, where roughness parameters peak at 4 hours, reflecting similar membrane interactions. At longer incubation times (24 hours), a decrease in roughness is observed in both cell lines, indicating AuNP internalization and a subsequent reduction in surface irregularities.

Larger AuNPs (50 nm and 70 nm) exhibit a similar roughness change pattern, with initial increases peaking at 4 hours. However, the

magnitude of the change is less pronounced compared to 20 nm AuNPs. Subsequently, a decrease in roughness is observed at 24 hours, indicating AuNP internalization. Notably, 70 nm AuNPs show a significant reduction in roughness at 24 hours, suggesting that cellular adaptation or AuNP agglomeration may reduce the effective interaction of particles with the cell surface.

The temporal dynamics of AuNP interaction reveal peak surface roughness at intermediate incubation times (around 4 hours), indicating optimal surface interaction and maximal membrane residence time. As the incubation time extends to 24 hours, roughness decreases, aligning with the AuNP internalization process [13]. This trend highlights a general mechanism across both cell lines and AuNP sizes: AuNPs initially reside on the cell membrane, increasing surface roughness, and later internalize, reducing surface irregularities. In A549 cells, roughness values peak at 4 hours of incubation, suggesting that the maximum nanoparticle-membrane interaction occurs within this window, likely due to the higher uptake efficiency of smaller, more flexible cancerous cells. In contrast, BEAS-2B cells show less dramatic changes in roughness, possibly due to their stiffer, more structurally stable membrane.

In this study, it was confirmed that cancerous cells, due to their distinct mechanical properties, exhibit more pronounced topographical changes upon interaction with AuNPs, which can be effectively captured through air-fixated AFM imaging. Importantly, these findings reinforce the potential of air fixation as an ideal preparation method for AFM studies, particularly when investigating membrane dynamics and surface roughness in cancer research. The compatibility of air fixation with AFM broadens its applicability in nanomedicine, providing a reliable alternative to more traditional preparation methods.

4. Conclusion

This study effectively demonstrates that interactions between AuNPs and cell membranes lead to significant topographical changes. Initially, surface roughness increases due to the presence of AuNPs on the cell membrane, and later decreases as internalization occurs. These

findings provide valuable insights into the behavior of AuNPs in biological environments, emphasizing the importance of controlling AuNP size and exposure duration to achieve desired cellular interactions.

Additionally, the results highlight the compatibility and advantages of air fixation for AFM sample preparation. Air fixation offers a balance of structural preservation and measurement stability, enabling precise topographical evaluation of AuNP interactions. This presents the potential for air fixation to become a valuable method for AFM studies, particularly in contexts where high-resolution, artifact-free imaging is critical.

Article Information Form

Acknowledgments

The author would like to thank University of Health Sciences, Experimental Medicine Application & Research Center, Validebag Research Park for Access to research infrastructure.

Funding

The author has not received any financial support for the research, authorship or publication of this study.

Author's Contribution

The author designed and conducted the experiments, wrote the original draft and the final version of the manuscript.

The Declaration of Conflict of Interest/ Common Interest

No conflict of interest or common interest has been declared by the author.

The Declaration of Ethics Committee Approval

This study does not require ethics committee permission or any special permission.

The Declaration of Research and Publication Ethics

The author of the paper declare that they comply with the scientific, ethical and quotation rules of SAUJS in all processes of the paper and that she does not make any falsification on the data collected. In addition, she declares that Sakarya

University Journal of Science and its editorial board have no responsibility for any ethical violations that may be encountered, and that this study has not been evaluated in any academic publication environment other than Sakarya University Journal of Science.

Copyright Statement

Author owns the copyright of her work published in the journal and her work is published under the CC BY-NC 4.0 license.

References

- [1] X. Deng, F. Xiong, X. Li, B. Xiang, Z. Li, X. Wu, C. Guo, X. Li, Y. Li, G. Li, W. Xiong, Z. Zeng, "Application of atomic force microscopy in cancer research," *Journal of Nanobiotechnology*, vol. 16, p. 102, 2018.
- [2] F. Xia, K. Youcef-Toumi, "Review: Advanced Atomic Force Microscopy Modes for Biomedical Research," *Biosensors*, vol. 12, Art. no. 12, 2022.
- [3] A. Massey, J. Stewart, C. Smith, C. Parvini, M. McCormick, K. Do & A. X. Cartagena-Rivera, "Mechanical properties of human tumour tissues and their implications for cancer development," *Nature Reviews Physics*, vol. 6, p. 269-282, 2024.
- [4] S. O. Konorov, H. G. Schulze, J. M. Piret, R. F. B. Turner, M. W. Blades, "Evidence of marked glycogen variations in the characteristic Raman signatures of human embryonic stem cells," *Journal of Raman Spectroscopy*, vol. 42, pp. 1135–1141, 2011.
- [5] M. M. Mariani, P. Lampen, J. Popp, B. R. Wood, V. Deckert, "Impact of fixation on in vitro cell culture lines monitored with Raman spectroscopy," *Analyst*, vol. 134, pp. 1154–1161, 2009.
- [6] B. Q. Huang, E. C. Yeung, "Chemical and Physical Fixation of Cells and Tissues: An Overview," in *Plant Microtechniques and Protocols*, E. C. T. Yeung, C. Stasolla, M. J. Sumner, B. Q. Huang, Eds., Cham: Springer International Publishing, 2015, pp. 23–43.
- [7] L. Andolfi, E. Bourkoula, E. Migliorini, A. Palma, A. Pucer, M. Skrap, G. Scoles, A.P. Beltrami, D. Cesselli, M. Lazzarino, "Investigation of Adhesion and Mechanical Properties of Human Glioma Cells by Single Cell Force Spectroscopy and Atomic Force Microscopy," *PLOS ONE*, vol. 9, p. e112582, 2014.
- [8] C. Huang, T. Ozdemir, L. C. Xu, P. J. Butler, C. A. Siedlecki, J. L. Brown & S. Zhang, "The role of substrate topography on the cellular uptake of nanoparticles," *Journal of Biomedical Materials Research Part B: Applied Biomaterials*, vol. 104, pp. 488-495, 2016.
- [9] J. Turkevich, P. C. Stevenson, J. Hillier, "A study of the nucleation and growth processes in the synthesis of colloidal gold," *Discussions of the Faraday Society*, vol. 11, pp. 55–75, 1951.
- [10] W. Haiss, N. T. K. Thanh, J. Aveyard, D. G. Fernig, "Determination of Size and Concentration of Gold Nanoparticles from UV–Vis Spectra," *Analytical Chemistry*, vol. 79, pp. 4215–4221, 007.
- [11] S. Suresh, "Biomechanics and biophysics of cancer cells," *Acta Biomaterialia*, vol. 3, pp. 413–438, 2007.
- [12] C. Lara-Cruz, J. J. Salazar, E. Ramón-Gallegos, P. Damian-Matsumura, N. Batina, "Increasing roughness of the human breast cancer cell membrane through incorporation of gold nanoparticles," *International Journal of Nanoscience*, vol. 11, pp. 5149–5161, 2016.
- [13] B. D. Chithrani, A. A. Ghazani, W. C. W. Chan, "Determining the Size and Shape Dependence of Gold Nanoparticle Uptake into Mammalian Cells," *Nano Letters*, vol. 6, pp. 662–668, 2006.